Type of the Paper (Article)

Tetramethylbenzidine: a photoacoustic probe for reactive oxygen species detection

Roger Bresolí-Obach [1,2], Marcello Frattini [1,3], Steffania Abruzetti [3,4], Cristiano Viappiani [3,4], Montserrat Agut [1] and Santi Nonell [1,*]

[1] Institut Químic de Sarrià, Universitat Ramon Llull, Via Augusta 390, 08017 Barcelona, Spain. roger.bresoliobach@kuleuven.be, mfrattini7@gmail.com, montserrat.agut@iqs.url.edu, santi.nonell@iqs.url.edu

[2] Current address: Department of Chemistry, Katholieke Universiteit Leuven, celestijnenlaan 200F, 3001 Heverlee (Leuven), Belgium.

[3] Dipartimento di Scienze Matematiche, Fisiche e Informatiche, Università di Parma, Parco Area delle Scienze 7A, 43124 Parma, Italy. stefania.abbruzzetti@unipr.it, cristiano.viappiani@unipr.it

[4] NEST, Istituto Nanoscienze, Consiglio Nazionale delle Ricerche, Piazza San Silvestro 12, 56127 Pisa, Italy.

* Correspondence: santi.nonell@iqs.url.edu; Tel.: +34-93-267-2000

Abstract: Photoacoustic imaging is attracting a great deal of interest owing to its distinct advantages over other imaging techniques such as fluorescence or magnetic resonance image. Availability of photoacoustic probes for reactive oxygen and nitrogen species (ROS/RNS) could shed light on a plethora of biological processes mediated by these key intermediates. Tetramethylbenzidine (TMB) is a non-toxic and non-mutagenic colorless dye that develops a distinctive blue color upon oxidation. In this work we have investigated the potential of TMB as photoacoustic probe for ROS/RNS. Our results indicate that TMB reacts with hypochlorite, hydrogen peroxide, singlet oxygen and nitrogen dioxide to produce the blue oxidation product, while ROS such as the superoxide radical anion, sodium peroxide, hydroxyl radical or peroxynitrite yield a colorless oxidation product. TMB does not penetrate *Escherichia coli* cytoplasm but is capable of detecting singlet oxygen generated in its outer membrane.

Keywords: 3,3′,5,5′-tetramethylbenzidine; reactive oxygen species (ROS); reactive nitrogen species (RNS); photoacoustic probes; optical sensors; singlet oxygen.

1. Introduction

Reactive oxygen species (ROS) are a family of oxygen-based molecules including singlet oxygen ($^1O_2$), superoxide radical anion ($O_2^{\bullet-}$), hydrogen peroxide (H_2O_2), hydroxyl radical ($^\bullet OH$) and peroxyl radical ($ROO^\bullet$), as well as hypochlorous acid and hypochlorite anion (HClO and ClO^-, respectively).[1] In low concentrations, ROS are adventitiously produced in several metabolic processes of aerobic organisms,[2] derived from molecular ground oxygen ($^3O_2$), and show high reactivity mainly as oxidant species. ROS oxidant effects are usually controlled by cell's own antioxidant defense mechanism.[3] However, when such processes are insufficient or overwhelmed, an accumulation of free ROS takes place inside cells, which are readily reactive towards proteins, nucleic acids and/or lipids.[4] Elevated ROS concentrations can lead to irreversible damage and eventually to cell death. In addition to ROS, reactive nitrogen species (RNS), present also a high oxidative reactivity towards biomolecules. RNS are a family of molecules derived from nitric oxide ($^\bullet NO$), such as nitrogen dioxide ($^\bullet NO_2$), nitrite (NO_2^-) or peroxynitrite ($ONOO^-$).[5] RNS can act alone or together with ROS to damage cells, mainly exerting nitrosative stress.[6] ROS and RNS can

 doi:10.20944/preprints202009.0536.v1

also be generated by light, whereby a photoexcited molecule can initiate a cascade of energy- or electron-transfer processes leading to the formation of ROS/RNS.[7] Medical technologies such as photodynamic therapy take advantage of this effect to locally eliminate cancerous cells or pathogenic microorganisms.[8,9]

Due to their important role in biological and medical processes, ROS/RNS detection techniques are required to monitor and quantify them with spatio-temporal resolution.[10] Currently available techniques can be broadly classified in two groups, one in which the analyte is directly monitored, e.g., $^1O_2$ through its near-infrared phosphorescence, or $O_2^{\bullet-}$ through electronic paramagnetic resonance,[11,12] or when the analyte reacts with some chemical probe which is then detected by suitable analytical techniques.[13] Direct techniques, while providing the advantage of specificity, lack in most cases the required sensitivity and require costly specialized equipment, which make the indirect approach more convenient and widespread, especially when conventional techniques such as absorption or fluorescence spectroscopy are used.[14,15] Several selective fluorescent probes for the detection of the most important ROS/RNS have been extensively developed and their use has been protocolized.[16] However, these optical techniques also present severe drawbacks when applied to biological systems, let alone living organisms, the main one is the poor penetration of light, e.g., in human tissue, and the strong scattering that prevent the detection of light emitted or reflected by deep targets.[17] These limitations can be circumvented using photoacoustic techniques, which provide deep tissue penetration.[18,19] For example, different internal organs such as liver, lung or brain have been imaged *in vivo* using photoacoustic techniques. Briefly, a dye in the excited state can release the absorbed radiation energy by radiative and/or non-radiative processes. The latter cause a local heating of the solution in the surroundings and thereby a local pressure and volume change (thermoelastic expansion), which could be detected with a microphone (e.g. piezoelectric detector).[20,21] The main advantage of detecting ultrasounds waves in comparison with visible light is that their propagation is less affected by absorption and/or cell scattering processes (or the tissue *in vivo*).

Recently, a few photoacoustic probes have been developed for the detection and imaging of biological relevant species (e.g. metal ions, pH, oxygen or oxidants).[22-26] In 2014, the first ROS photoacoustic nanosensor was developed by embedding a cyanine 7 derivative to a semiconductive polymeric nanoparticle.[27] Since then a few more examples of photoacoustic nanosensors have been developed for ROS/RNS detection (e.g. a photoactivatable, reversible or theragnostic photoacoustic nanosensor among others).[28-30] In all these published works, fluorescent dyes are used as photoacoustic reporters. This seems far from efficient because fluorescent dyes have been engineered to optimize their emissive properties, which detracts from the efficiency of non-radiative decay processes that underline the photoacoustic signal.

An ideal photoacoustic probe should fulfill a series of requirements: i) it should have high molar absorption coefficient, ii) it should release all the absorbed energy as heat as fast as possible and iii) it should have high photobleaching resistance.[31] Taking into account the presented requirements, we performed a bibliographic research in order to reprofile some existent dyes, which are highly reactive against ROS and meet such requirements. 3,3′,5,5′-Tetramethylbenzidine (TMB) is a non-colored, non-toxic and non-carcinogenic compound that reacts with some ROS generating a blue oxidized complex.[32-34] TMB is currently used as visualizing reagent in ELISA assays, taking advantage of its oxidation with H_2O_2 in presence of horseradish peroxidase.[35]

Preprints (www.preprints.org) | NOT PEER-REVIEWED | Posted: 23 September 2020 doi:10.20944/preprints202009.0536.v1

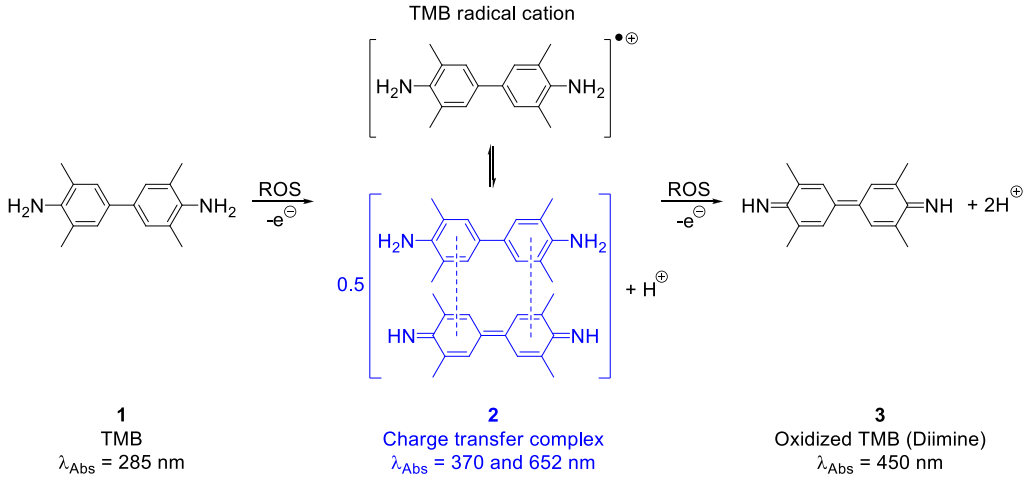

Scheme 1. TMB reactivity towards oxidant agents.

As it can be seen in Scheme 1, in a first step, TMB reacts with an oxidant agent to yield a radical cation ($TMB^{\bullet+}$), which forms a blue (λ_{abs} = 652 nm) charge transfer complex (**2**) with a second TMB molecule. In some cases, the presence of additional oxidizing agent leads to a diimine product (**3**), which has a yellow coloration (λ_{abs} = 450 nm).[32,34,36] Finally, with a large excess of oxidizing agent, the reaction will proceed to yield other non-colored oxidized derivatives. In this work we have assessed the potential of TMB as photoacoustic probe for ROS/RNS using laser induced optoacoustic spectroscopy (LIOAS). We have studied its reactivity towards different ROS/RNS in water ad have used it to detect $^1O_2$ generated in *Escherichia coli* cells.

2. Materials and Methods

2.1. Materials

3,3′,5,5′-Tetramethylbenzidine (TMB), sodium hypochlorite solution (50 g/l in H_2O; NaClO), potassium superoxide (KO_2), Rose Bengal (RB), 2,2,6,6-tetramethylpiperidin-1-yl)oxyl (TEMPO), sodium azide (NaN_3), bromocresol purple (BCP) and phosphate buffered saline (PBS; pH = 7.4) were purchased from Sigma-Aldrich (St. Louis, MO, USA). Hydrogen peroxide solution (30 wt % in H_2O; H_2O_2), sodium nitrite ($NaNO_2$), sodium nitroprusside ($Na_2[Fe(CN)_5NO]$) and Luria–Bertani (LB) medium were supplied by Panreac (Barcelona, Spain). 5-mono(N-decyl-4-pyridyl)-10,15,20-tri(N-methyl-4-pyridyl)-21H,23H-porphine tetrachloride (MDPyTMPyP) were supplied by Frontier Scientific (Logan, UT, USA). All reagents were used as received.

2.2. General spectroscopic measurements

All spectroscopic measurements were carried out in 1-cm quartz cuvettes (Hellma, Germany) at room temperature. Absorption spectra were recorded on a Cary 6000i spectrophotometer (Varian, Palo Alto, CA, USA).

The time-resolved photoacoustic signals were recorded using a home-built LIOAS equipment. TMB was excited using a Q-switched Nd:YAG laser (Surelite I-10, Continuum, CA, USA) coupled to an OPO laser (SL OPO, 5 ns pulse width, 10-100 μJ per pulse, Continuum, CA, USA). The excitation wavelengths were 652 nm or 450 nm depending on the experiment. The laser power was varied using neutral density filters. The laser beam was passed through a vertical slit of dimensions 5x1 mm immediately before entering the cuvette. Then, the laser-induced pressure changes in the sample were detected by a Panametrics piezoelectric transducer pressed to the side wall of a cuvette and held in a temperature-controlled holder (Quantum Northwest, WA, USA). A thin layer of silicon grease (Baysilone-35, Bayer, Leverkusen, Germany) ensured optimum acoustic coupling between

 doi:10.20944/preprints202009.0536.v1

the cuvette and the piezoelectric transducer. After amplification, the signal was fed to a Lecroy Wavesurfer 454 oscilloscope (Teledyne LeCroy, VA, USA) for digitizing and averaging (typically 1000 shots) and finally transferred to a PC for data storage and analysis. The amplitude of photoacoustic signal maximum (H_{max}) is proportional to the absorbed laser energy, and therefore to the energy of the laser pulse (E) and the sample absorption factor by (1).

$$H_{max} = k'\emptyset[1 - 10^{-A}] \quad (1)$$

Where k' is a proportional constant that accounts for electronic and geometric factors of the experimental system and ϕ is the *photoacoustic efficiency*.[37] In optically-thin samples, the absorption factor is proportional to the concentration of the absorber (c), which can be taken advantage of for absorber quantification purposes. Thus, Equation (1) can be simplified to Equation (2):

$$H_{max} \sim k''\emptyset c \quad (2)$$

The ϕ value is determined by comparing H_{max} for optically-matched solutions of the sample and a suitable photoacoustic reference (BCP dissolved in 0.1 M NaOH, with ϕ = 1, was used in this work,)[38] as indicated in Equation (3).

$$\emptyset_{Sample} = \frac{H_{max;Sample}}{H_{max;Ref}}\emptyset_{Ref} \quad (3)$$

2.3. Statistical analysis

The limit of detection (LOD) and the limit of quantification (LOQ) were calculated as 3- and 10-fold the standard deviation of the blank interpolated to the analyte calibration curve. The standard deviation of the blank was obtained from ten independent blank samples.

2.4. Sources of the ROS and RNS tested

The different ROS and RNS used in this work were prepared according to the protocols below. Sodium hypochlorite (NaOCl) was diluted from the commercial source (50 g/L of NaClO in water). Superoxide anion radical ($O_2^{\bullet-}$) was added as solid KO_2. Hydrogen peroxide (H_2O_2) was diluted from the commercial source (H_2O_2 30% in water). Hydroxyl radical ($^{\bullet}OH$) was generated by irradiation of 10 mM $NaNO_2$ solution with UV-A light (354 ± 20 nm).[39] Generation of $^{\bullet}OH$ was verified by scavenging it with terephthalic acid and mannitol (Figure S1; Schemes S1 and S2).[40] Singlet oxygen ($^1O_2$) was generated by irradiation of Rose Bengal (a well-known $^1O_2$ photosensitizer)[41] with green light (520 ± 18 nm). Nitric oxide ($^{\bullet}NO$) was generated from the thermal decomposition of an aqueous solution of 1 M sodium nitroprusside ($Na_2[Fe(CN)_5NO]$).[42] Peroxynitrite anion ($ONOO^-$) was generated as described in ref.[43] Briefly, 1.5 M NaOH (aq) was added to a mixture of 0.6 M $NaNO_2$, 0.7 M H_2O_2 and 0.6 M HCl. The $ONOO^-$ solution was used immediately after its preparation. Nitrogen dioxide ($^{\bullet}NO_2$) was generated from the decomposition of sodium nitrite ($NaNO_2$).[44] Briefly, 1 M $NaNO_2$ solution was added to H_2SO_4 (96%) and the generated brownish gas was collected in a balloon and injected into a sealed cuvette containing the TMB solution. Nitrite (NO_2^-) was diluted from a 1 M sodium nitrite solution. 2,2,6,6-Tetramethylpiperidin-1-yl)oxyl (TEMPO) was added as solid.

2.5. Bacterial cell cultures

2.5.1. *Escherichia coli* cells with the endogenous PS miniSOGs

E. coli cells (DH10β, Invitrogen, CA, USA) were transformed with the expression vector encoding the fluorescent proteins miniSOG wt, miniSOG Q103L and miniSOG Q103V. Cells were grown aerobically from a single colony to an OD_{600} = 0.3 in Luria–Bertani (LB) medium supplemented with 100 μg/mL ampicillin at 37°C. Untransformed DH10β cells were grown in LB without ampicillin. Protein expression was induced by addition of 0.2% (w/v) L-arabinose. Cells

Preprints (www.preprints.org) | NOT PEER-REVIEWED | Posted: 23 September 2020 doi:10.20944/preprints202009.0536.v1

were harvested by centrifugation after 3 hours. Afterwards the cells were incubated with TMB (200 μM) for 10 minutes and washed three times with PBS (pH 7.4).

2.5.2. *Escherichia coli* cells with the exogenous PS MDPyTMPyP

E. coli cells (ATCC 25922, Manassas, VA, USA) were grown aerobically from a single colony to an OD_{600} = 0.3 in LB medium at 37 °C. Then, cells were harvested by centrifugation and washed three times with PBS (pH 7.4). Afterwards, cells were incubated with MDPyTMPyP (10 μM), TMB (200 μM) and NaN_3 (if it was necessary; 50 mM) for 10 minutes, followed by three washes with PBS (pH 7.4).

3. Results

*3.1. Photoacoustic and spectroscopic properties of TMB and its oxidation products (**2** and **3**)*

The absorption spectra of TMB, the blue complex **2**, and the yellow diimine **3** in PBS are shown in Figure 1A. TMB absorbs only in the ultraviolet region with a band centered at 290 nm. Upon addition of NaClO, we observed the formation of the blue complex **2**, which absorbs throughout the visible spectrum with bands at 650, 460 and 370 nm. When a light excess of NaClO relative to TMB was added, the blue complex **2** evolved to the yellow diimine **3**, which shows a single absorption band at 450 nm. Further addition of NaClO oxidized **3** to uncolored products.

Based on the absorption spectra of TMB, **2** and **3**, we chose 652 nm for probing **2** and 450 nm for probing **3** in the photoacoustic experiments. A clear photoacoustic signal at 652 nm appeared upon addition of NaClO, which we ascribe to the formation of **2** (Figure 1B). The amplitude of the photoacoustic signal increased up to a maximum and then began to decrease, indicating the disappearance of **2**. Two factors contribute to this: as oxidation proceeds, there is less and less TMB available to form the complex **2**, resulting in the saturation of the signal at [NaClO] ~ 250 μM. In addition, $TMB^{\bullet+}$ is further oxidized to the diamine **3**, which was demonstrated by the concomitant growth of the photoacoustic signal at 450 nm and its decrease at 652 nm at high [NaClO] (Figure 1B inset).

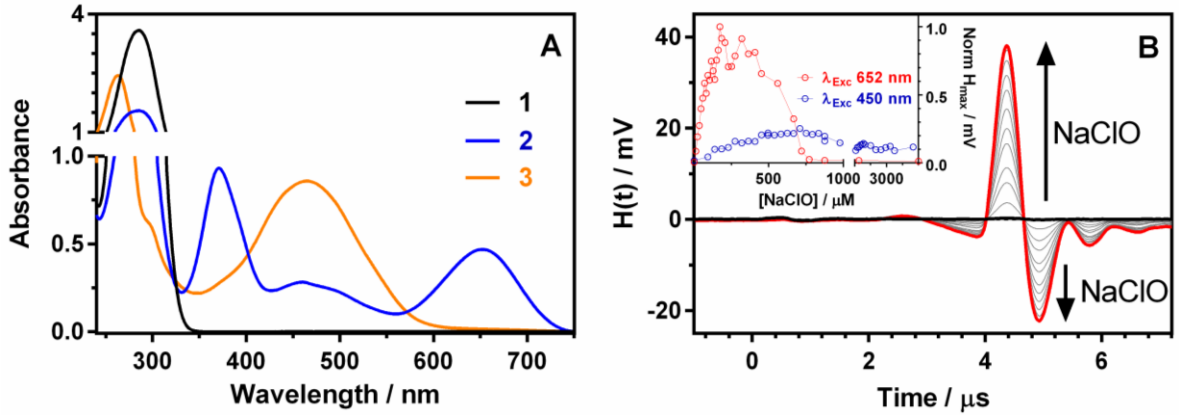

Figure 1. (A): Absorption spectra of TMB, **2** and **3** in PBS. (B): TMB photoacoustic waveforms enhancement upon successive NaClO additions in PBS ([TMB] = 200 μM; [NaClO] = 0-150 μM; λ_{exc} = 652 nm). Inset: Photoacoustic maximum amplitude in function of the amount of NaClO added. The excitation wavelengths were 652 (**2**; red line) and 450 (**3**; blue line) nm. [TMB] = 200 μM.

3.2. Factors affecting the photoacoustic signal

The amplitude of the photoacoustic signal reflects the amount of heat deposited in the system through radiationless decay of the excited states, as well as the differences in molecular volumes between the excited- and the ground-state species. Comparing the amplitude of the photoacoustic signal for **2** with that of the photocalorimetric reference BCP, the photoacoustic efficiency of **2** was

Preprints (www.preprints.org) | NOT PEER-REVIEWED | Posted: 23 September 2020 doi:10.20944/preprints202009.0536.v1

determined as ϕ = 0.95 ± 0.10 (Figure 2A). Kinetic analysis of time-resolved photoacoustic signal revealed that the excited state decay of **2** is faster than the temporal-resolution of the technique. Finally, **2** was found to be non-fluorescent. These results indicate that **2** is an ideal photoacoustic probe since it releases fast and efficiently as heat all the absorbed light energy. In addition, the photoacoustic signal increases linearly with the excitation laser power (Figure S2) and is fairly photostable, since 8500 laser shots of 100 µJ are needed to reduce the signal by half (Figure S3), while to obtain a decent signal 10 shots of 10 µJ suffice.

Next, the effect of the TMB concentration was examined. The highest photoacoustic amplitude was observed when two equivalents of TMB reacted with one equivalent of NaClO, therefore this proportion was kept for all experiments. A linear increase of the photoacoustic signal amplitude with TMB was observed up to roughly 30 µM and the signal leveled off around 200 µM (Figure S4) in agreement with Equation (1). Monitoring of **2** enables measurements of NaClO concentration up to 100 µM. H_{max} increases linearly with NaClO up to a concentration of 15 µM (Figure 2B). The precision of the method has been assessed using 10 independent replicates obtaining a standard deviation of 15% (Figure S5), which is in accordance with typical standard deviation values for LIOAS. The detection and quantification limits have then been estimated as 0.6 and 1.4 µM respectively (Figure S6).

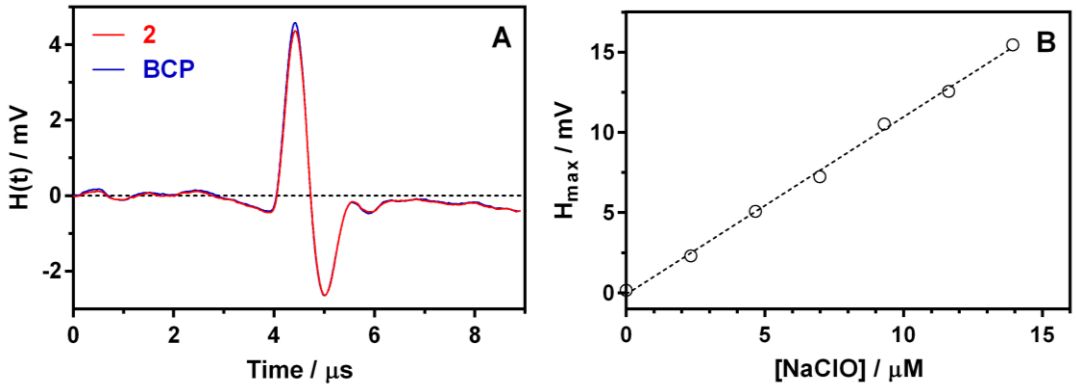

Figure 2. Determination of ϕ for **2** (red line) in PBS (pH 7.4). The reference photoacoustic wave was obtained using an optically-matched bromocresol purple solution (BCP; ϕ = 1 (0.1 M NaOH); blue line)[37] at the excitation wavelength (λ_{Exc} = 652 nm). (B): Photoacoustic maximum amplitude vs concentration of NaClO added in PBS (pH 7.4). [TMB] = 200 µM; λ_{exc} = 652 nm.

3.3. TMB reactivity towards the tested ROS, RNS and TEMPO

After establishing the spectroscopic and photoacoustic properties of TMB, **2** and **3**, we determined the reactivity of TMB towards other ROS, RNS and the stable free radical TEMPO (Figure 3). Thus, TMB was allowed to react with them for 5 minutes before the photoacoustic response was recorded. For TEMPO and the stable ROS/RNS, we recorded the photoacoustic response at oxidant:TMB ratios ranging from 1:20 up to 10:1 eq, whereas for oxidants generated photochemically, we evaluated the photoacoustic response as a function of the irradiation time. When a species would not show any photoacoustic signal, we repeated the experiment in the presence of 100 µM ClO^- as a control. The results are summarized in Scheme 2. Three types of response were observed:

Preprints (www.preprints.org) | NOT PEER-REVIEWED | Posted: 23 September 2020 doi:10.20944/preprints202009.0536.v1

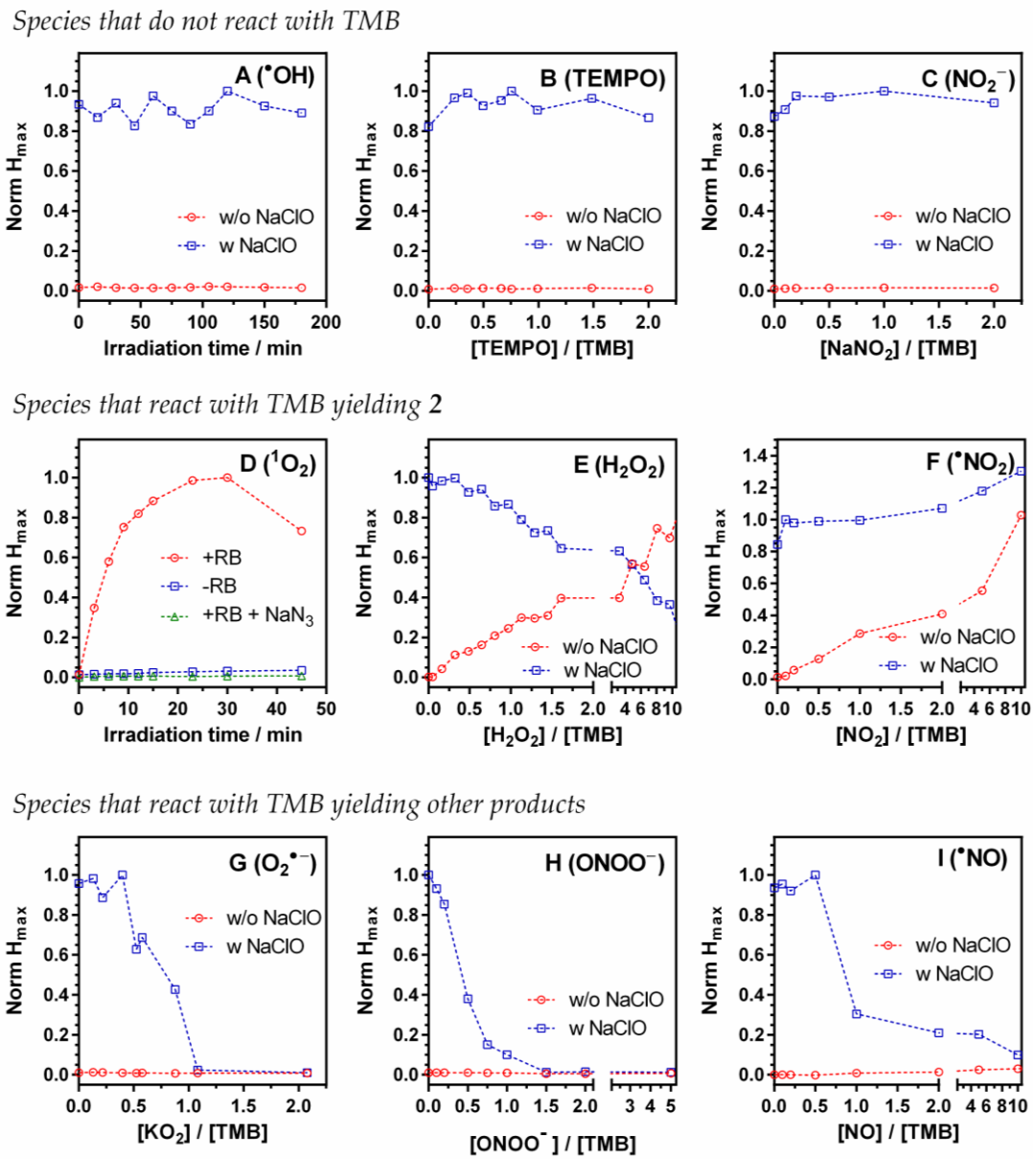

Figure 3. Photoacoustic maximum amplitude of TMB after reacting with different ROS and RNS. (A): Hydroxyl radical (•OH) generated via sodium nitrite photolysis in water (λ_{exc} = 354 ± 20 nm). (B): (2,2,6,6-Tetramethylpiperidin-1-yl)oxyl (TEMPO). (C): Sodium nitrite ($NaNO_2$). (D): Singlet oxygen ($^1O_2$) generated via Rose Bengal irradiation (λ_{exc} = 520 ± 18 nm). (E): Hydrogen peroxide (H_2O_2). (F): Nitrogen dioxide (NO_2) generated via sodium nitrite acid decomposition. (G): Superoxide radical anion ($O_2^{\bullet-}$). (H): Peroxynitrite ($ONOO^-$). (I): Nitric oxide (NO) generated via sodium nitroprusside decomposition. As control for B, C, E, F, G, H after the acquisition of the photoacoustic signal, 100 µM NaClO was added and their photoacoustic signal measured again (red and blue line respectively).

3.3.1. Species that give no photoacoustic signal

This was the case for •OH, TEMPO and $NaNO_2$ (Figure 3, panels B, F, J). TEMPO and $NaNO_2$ did not react with TMB under these conditions. It is well known that nitrous acid HNO_2 reacts with aromatic amines to form diazonium salts and leading eventually to the formation of colored diazo compounds. However, the pK_a of HNO_2 is 3.15, therefore this reaction is not expected to occur at physiological pH.[45] The reduction potential of nitrite is 0.375 V vs NHE,[46] while the reduction potential of the **2** is +0.553 V,[47] therefore production of **2** is not favorable. TEMPO has a very similar reduction potential (+0.380 V),[48] therefore no reaction is to be expected either. On the other hand, TEMPO may also react abstracting a hydrogen from TMB, however the extent of this reaction

Preprints (www.preprints.org) | NOT PEER-REVIEWED | Posted: 23 September 2020 doi:10.20944/preprints202009.0536.v1

seems to be negligible under our experimental conditions. Surprisingly, $^{\bullet}OH$ does not react with TMB despite having a most favorable reduction potential.[49] In general, $^{\bullet}OH$ reactions tend to be diffusion-controlled owing to their strong reactivity. Indeed, $^{\bullet}OH$ reacts with TPA at the same concentration used for TMB (200 μM; Figure S1). As a final control, we added 100 μM ClO^- to the analyzed solution and repeated the measurement. Reassuringly, the extent of production of **2** was the same in the absence and in the presence of $^{\bullet}OH$. The same holds true for TEMPO and $NaNO_2$.

3.3.2. Species that react with TMB yielding **2**

In addition to ClO^- (Figure 1), **2** was formed in the presence of H_2O_2 (+0.80 V), $^1O_2$ (+0.81 V), and $^{\bullet}NO_2$ (+1.04 V), which have sufficiently high reduction potentials for oxidizing TMB (Figure 3, panels C, E, I).[49] The photoacoustic signal increases in an almost linear fashion with the concentration of H_2O_2, although the maximum amplitude is not reached until a H_2O_2:TMB ratio of about 15. This most likely indicates that the reaction with TMB is slow. Bearing in mind the prospective use of TMB for measurements in biological samples, we ruled out extending the time lag between TMB addition and measurement as well as the addition of accelerators such as horseradish peroxidase. Addition of 100 μM ClO^- to the analyzed solutions produced a signal that decreased with the concentration of H_2O_2 in a complementary fashion to the increase observed in its absence. In fact, the sum of the signals before and after addition of ClO^- is approximately 100% in all cases. This indicates that ClO^- oxidizes the TMB that did not react H_2O_2, adding to the signal. Alternative reactions between ClO^- and H_2O_2, e.g., the production of $^1O_2$ [50] cannot be ruled out.

Figure 3E shows that $^1O_2$, generated by irradiation of RB with green light, reacts readily with TMB to produce the blue complex. The photoacoustic signal shows a concentration dependence very similar to that of ClO^-, namely a steady growth until a plateau value is reached, followed by a decrease when the number of free TMB molecules is insufficient to form the complexes with all produced $TMB^{\bullet+}$. The signal disappeared when the TMB solution was exposed to green light in the absence of RB and when 10 mM sodium azide, a well-known $^1O_2$ quencher,[51] was added, indicating that that the formation of the blue complex **2** is indeed due to reaction of TMB with $^1O_2$.

The final oxidant in this group, $^{\bullet}NO_2$, shows a behavior very similar to that of H_2O_2 (Figure 3I). It reacts with TMB to yield the blue complex **2** and the reaction is not yet complete when the photoacoustic signal is recorded, unless $^{\bullet}NO_2$ is added in a 10-fold excess. Unlike H_2O_2, addition of ClO^- gives the 100% signal system and even rises above this level at the highest $^{\bullet}NO_2$ concentrations, most likely due light absorption by $^{\bullet}NO_2$ itself ($\sigma_{650} = 1.54 \times 10^{-20}$ cm^2/molecule; gas phase).[52]

3.3.3. Species that react with TMB yielding non colored products

This was the case of $O_2^{\bullet-}$, $ONOO^-$ and $^{\bullet}NO$, which did not form the blue charge-transfer complex **2** at any concentration or produced only minute amounts of it (Figure 3 panels A, D, H). As in the case of $^{\bullet}OH$, this was surprising because the reduction potentials are very favorable (for $O_2^{\bullet-}$, +1.46 V, and for $ONOO^-$, +1.20 V); less so for $^{\bullet}NO$, -0.15 V.[49,53] Unlike the observations made for $^{\bullet}OH$, subsequent addition of NaClO did not produce the 100% photoacoustic signal but a signal that decreased with the initially-added concentration of the ROS/RNS as in the H_2O_2 case. This indicates that TMB had actually been consumed, however yielding products different than **2**. Since our goal was to assess the usefulness of TMB as a photoacoustic probe for ROS/RNS, we did not seek to investigate the nature of such products. Nevertheless, a possible explanation for the strong oxidants $O_2^{\bullet-}$ and $ONOO^-$ is that TMB was oxidized to the diamine **3.** In addition, it has been reported that $O_2^{\bullet-}$ can oxidize aniline (taken as a simple TMB model) to their correspondent nitro or nitroso derivatives [54] as well as to 4-nitro-N-phenylaniline.[55] Similarly, $ONOO^-$ and $^{\bullet}NO$ can react with primary and secondary amines to yield N-nitrosamines and N-nitramines.[56] As a final note, it is worth noting, that for high concentration of $^{\bullet}NO$ (20- and 30-eq.) a small amount of TMB is oxidized to yield **2**, confirming the minor contribution of the electron-transfer reaction pathway .

Preprints (www.preprints.org) | NOT PEER-REVIEWED | Posted: 23 September 2020 doi:10.20944/preprints202009.0536.v1

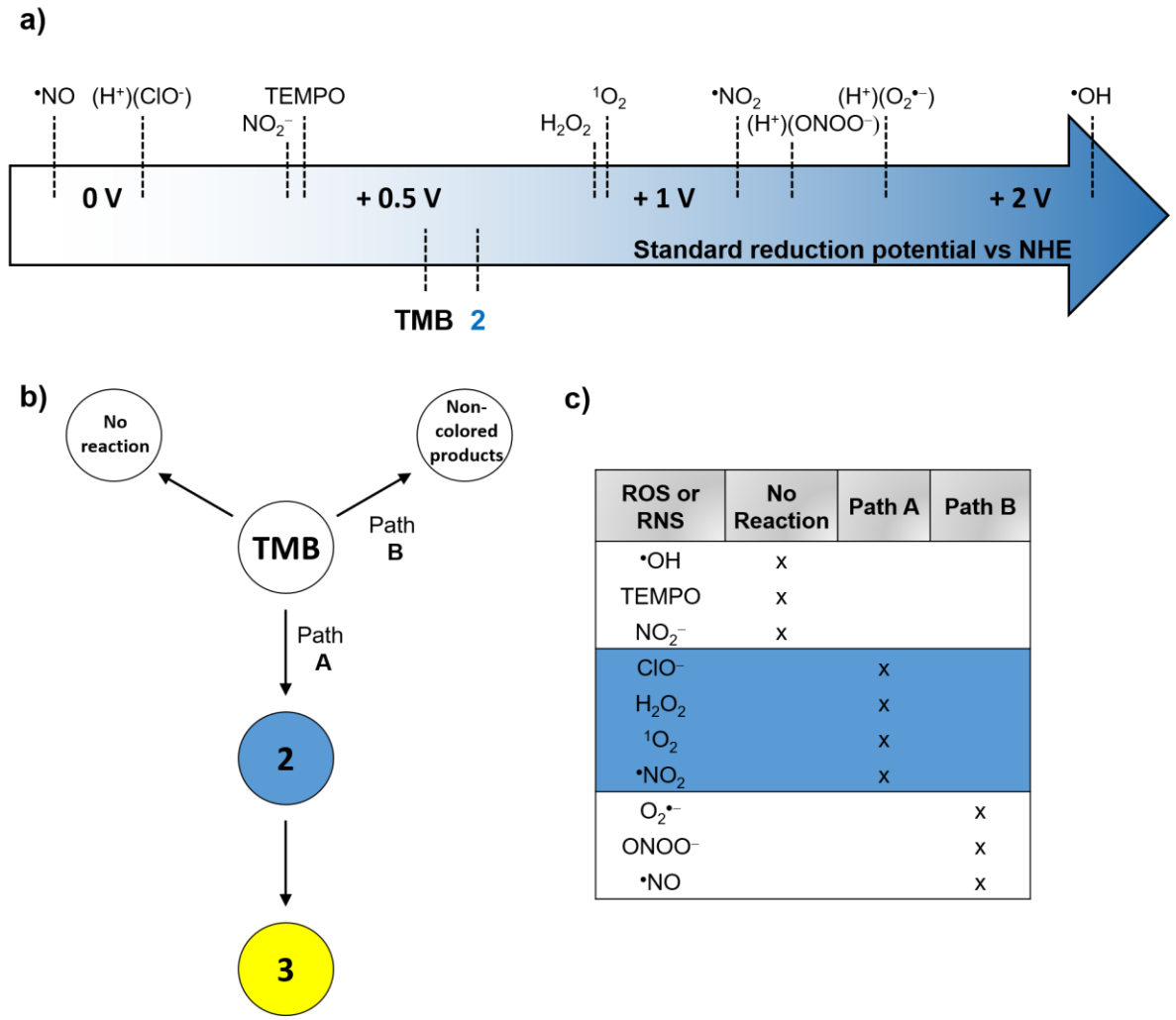

ROS or RNS	No Reaction	Path A	Path B
•OH	x		
TEMPO	x		
NO_2^-	x		
ClO^-		x	
H_2O_2		x	
$^1O_2$		x	
$•NO_2$		x	
$O_2•^-$			x
$ONOO^-$			x
•NO			x

Scheme 2. (a) Standard reduction potentials for the different tested ROS, RNS, TEMPO and TMB.[46-49,53] (b) The possible reaction pathways of TMB towards different ROS or RNS. (c) Table summarizing the reactivity towards TMB of the different ROS and RNS studied. In addition, for the cases that photoacoustic signal can be detected (path A) limits of detection and quantification have been calculated (LOD and LOQ respectively).

3.3. Detection of ROS in biological media

In the previous section we established that TMB is a useful photoacoustic probe for ClO^- and $^1O_2$ and, to a lesser extent, also for H_2O_2 and $•NO_2$. We then sought to assess its performance in biological media. To this end, we added TMB to suspensions of *wt* DH10β *Escherichia coli* bacteria as well as three genetically-modified strains that express the ROS photosensitizing proteins miniSOG and its mutants Q103V and Q103L, respectively. These are flavin-binding proteins that produce $^1O_2$ and other ROS in different proportions under exposure to blue light (460 nm).[57-59] All strains produced a photoacoustic signal at 652 nm, likely due to light absorption by heme. However the signal was not enhanced upon exposure of the bacteria to blue light (Figure 4A and Figure S7). This indicates that no blue complex is formed, which may be due to TMB and the ROS being in distant cellular locations. Since the photosensitizing proteins are located in the cytoplasm, the most likely explanation is that TMB is not internalized by the bacteria. To confirm this, we conducted a second experiment in which the *E. coli* ATCC 25922 bacterial cells were incubated with the porphyrin MDPyTMPyP (Scheme S3), which accumulates in the bacterial outer membrane.[60] In this case, a clear enhancement was observed upon exposure to 420 nm blue light, confirming the formation of the blue complex **2** (Figure 4B and Figure S8). No enhancement was observed in the absence of MDPyTMPyP. We next addressed the question whether TMB binds to the bacteria or remains in the

Preprints (www.preprints.org) | NOT PEER-REVIEWED | Posted: 23 September 2020 doi:10.20944/preprints202009.0536.v1

bulk solution. When we centrifuged the suspension and recorded the photoacoustic signal of the supernatant solution, no signal could be observed. However, we could recover it by resuspending the bacterial pellet (Figure S9). This indicates that TMB binds strongly to bacterial cells, but is not internalized by them. As a final experiment, we observed that adding 50 mM NaN_3 prevented the signal enhancement,[51] confirming that $^1O_2$ was the ROS responsible for TMB oxidation.

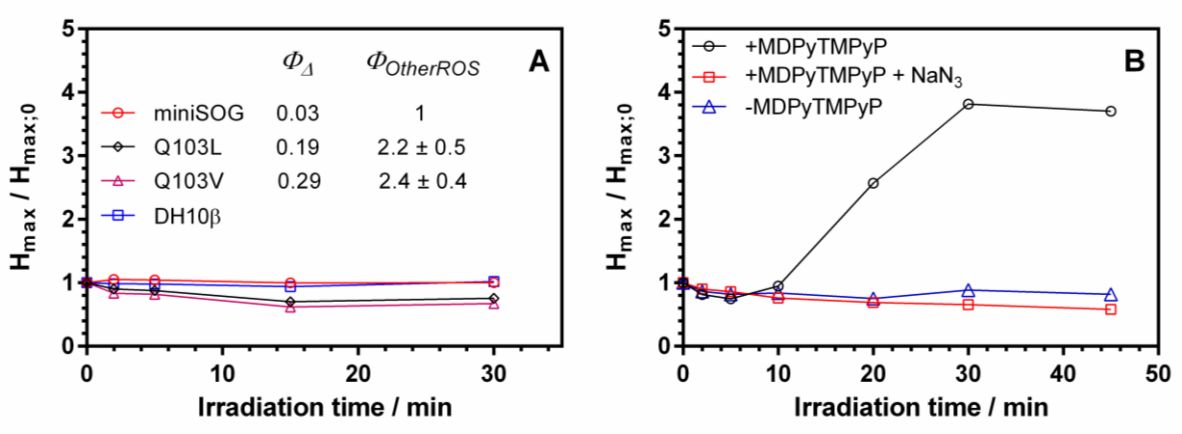

Figure 4. Photoacoustic maximum amplitude enhancement of TMB for: (A) untransformed DH10β (blue squares) and miniSOG-expressing (red circles, black rhombuses and magenta triangles for miniSOG, miniSOG Q103L and miniSOG Q103V respectively) *E. coli* cells for different irradiation times (lamp power 14.0 mW/cm^2; λ_{Irr} = 459 ± 10 nm). The values of $^1O_2$ quantum yield (Φ_Δ) and relative generation of other ROS ($\Phi_{OtherROS}$) by miniSOG and its mutants Q103L and Q103V are taken from ref. [59]. (B): *E. coli* ATCC 25922 cells in the presence (200 μM; black circles) and absence (blue triangles) of MDPyTMPyP for different irradiation times (lamp power 5.5 mW/cm^2; λ_{Irr} = 420 ± 20 nm). Control experiment was realized coincubating MDPyTMPyP with 50 mM NaN_3 (red squares).

Closer inspection of the time evolution of the photoacoustic signal reveals a time lag between the beginning of irradiation and the onset of the signal. This behavior has been observed also for fluorescent ROS probes in cells and is believed to reflect the scavenging of the first waves of $^1O_2$ by cellular antioxidants.[61] When these are consumed, TMB oxidation proceeds.

4. Conclusions

Photoacoustic probes circumvent the main limitations of fluorescent probes, particularly tissue penetration and the need for transparent media. In addition, they can report in a depth-resolved manner taking advantage of the lower speed of propagation compared to light. We have demonstrated that the chromogenic TMB is a suitable photoacoustic probe for red-light monitoring of ClO^-, $^1O_2$ and, to a lesser extent, H_2O_2 and $^\bullet NO_2$ due to the formation of a blue complex upon oxidation. Other ROS/RNS either do not react with TMB at any appreciable rate ($^\bullet OH$, NO_2^- and the TEMPO radical) or yield photoacoustically-silent products ($O_2^{\bullet-}$, $ONOO^-$ and $^\bullet NO$). TMB binds to the outer membrane of *E. coli* bacterial cell wall and aptly reports on $^1O_2$ located in its vicinity. The results of this work may pave the way to the development of new probes for photoacoustic imaging of a wide variety of biologically-relevant species, thereby providing a sensitive and selective alternative to fluorescence imaging.

Supplementary Materials: The following are available online at www.mdpi.com/xxx/s1, Figure S1: Reactivity of terephtalic acid towards $^\bullet OH$. Figure S2: Laser energy dependence of photoacoustic maximum amplitude for **2**. Figure S3: Photostability of **2** upon 652 nm laser-pulsed irradiation. Figure S4: Photoacoustic maximum amplitude for **2** in function of the initial TMB concentration upon reaction with ClO^-. Figure S5: Precision test. Figure S6: Limit of detection and limit of quantification test. Figure S7: Photoacoustic waveforms for different *E. coli* cell-suspension encoding different ROS generating proteins (miniSOG, miniSOG Q103L,miniSOG Q103V) as a function of the irradiation time. Figure S8: Photoacoustic waveforms for *E. coli* cell-suspension incubated with or without 10 μM MDPyTMPyP as a function of the irradiation time. Figure S9: Photoacoustic waveforms for the supernatant and the pellet resuspension for *E. coli* cell-suspension incubated with 10 μM MDPuTMPyP

and irradiated during 45 minutes. Scheme S1: Reactivity of terephtalic acid towards •OH. Scheme S2: Photolysis of $NaNO_2$ in an aqueous environment to generate •OH. Scheme S3: Chemical structure of MDPyTMPyP.

Author Contributions: Conceptualization: R.B.-O. and S.N.; methodology: R.B.-O. and S,N..; validation: R.B.-O. and S.N.; formal analysis: R.B.-O.; investigation: R.B.-O. and M.F.; resources: S.A., C.V., M.A. and S.N.; data curation: R.B.-O. and S.N.; writing—original draft preparation: R.B.-O. and S.N..; writing—review and editing: R.B.-O., M.F., S.A. C.V., M.A. and S.N..; visualization: R.B.-O. and S.N.; supervision: S.N..; project administration: S.N..; funding acquisition: S.N. All the authors have read and agreed to the published version of the manuscript.

Funding: This research was funded by Ministerio de Economía y Competitividad (grant number CTQ2016-78454-C2-1-R), the European Social Funds and the SUR del DEC de la Generalitat de Catalunya (grant number 2017 FI_B2 00140) and the Vlaanderen Fonds Wetenschappelijk Onderzoek (grant number 12Z8120N). M.F. was recipient of an Erasmus+ traineeship.

Conflicts of Interest: "The authors declare no conflict of interest."

References

1. Krumova, K.; Cosa, G. Overview of Reactive Oxygen Species. In Singlet Oxygen: *Applications in Biosciences and Nanosciences*, 1st ed.; Nonell, S., Flors, C., Eds.; RSC: London, United Kingdom, 2016, Volume 1, pp. 1-21.

2. Halliwell, B. Reactive species and antioxidants. Redox biology is a fundamental theme of aerobic life. *Plant Physiol.* **2006**, *141*, 312–322.

3. Birben, E.; Sahiner, U.M.; Sackesen, C.; Erzurum, S.; Kalayci, O. Oxidative Stress and Antioxidant Defense. *World Allergy Organ. J.* **2012**, *5*, 9–19.

4. Schieber, M.; Chandel, N.S. ROS Function in Redox Signaling and Oxidative Stress. *Curr. Biol.* **2014**, *24*, R453–R462.

5. Patel, R.P.; McAndrew, J.; Sellak, H.; White, C.R.; Jo, H.; Freeman, B.A.; Darley-Usmar, V.M. Biological aspects of reactive nitrogen species. *Biochim. Biophys. Acta* **1999**, *1411*, 385–400.

6. Corpas, F.J.; Barroso, J.B. Nitro-oxidative stress vs oxidative or nitrosative stress in higher plants. *New Phytol.* **2013**, *199*, 633–635.

7. Foote, C.S. Definition of type I and type II photosensitized oxidation. *Photochem. Photobiol.* **1991**, *54*, 659.

8. Agostinis, P.; Berg, K.; Cengel, K.A.; Foster, T.H.; Girotti, A.W.; Gollnick, S.O.; Hahn, S.M.; Hamblin, M.R.; Juzeniene, A.; Kessel, D.; Korbelik, M.; Moan, J.; Mroz, P.; Nowis, D.; Piette, J.; Wilson, B.C.; Golab, J. Photodynamic therapy of cancer: An update. *CA. Cancer J. Clin.* **2011**, *61*, 250–281.

9. Wainwright, M.; Maisch, T.; Nonell, S.; Plaetzer, K.; Almeida, A.; Tegos, G.P.; Hamblin, M.R. Photoantimicrobials—are we afraid of the light? *Lancet Infect. Dis.* **2017**, *17*, e49–e55.

10. Winterbourn, C.C. Reconciling the chemistry and biology of reactive oxygen species. *Nat. Chem. Biol.* **2008**, *4*, 278–286.

11. Jiménez-Banzo, A.; Ragàs, X.; Kapusta, P.; Nonell, S. Time-resolved methods in biophysics. 7. Photon counting vs. analog time-resolved singlet oxygen phosphorescence detection. *Photochem. Photobiol. Sci.* **2008**, *7*, 1003–1010.

12. Yu, J.; Chen, J.; Li, C.; Wang, X.; Zhang, B.; Ding, H. ESR signal of superoxide radical anion adsorbed on TiO_2 generated at room temperature. *J. Phys. Chem. B* **2004**, *108*, 2781–2783.

13. Chen, X.; Wang, F.; Hyun, J.Y.; Wei, T.; Qiang, J.; Ren, X.; Shin, I.; Yoon, J. Recent progress in the development of fluorescent, luminescent and colorimetric probes for detection of reactive oxygen and nitrogen species. *Chem. Soc. Rev.* **2016**, *45*, 2976–3016.

14. Nosaka, Y.; Nosaka A.Y. Generation and detection of reactive oxygen species in photocatalysis. *Chem. Rev.* **2017**, *117*, 11302-11336.

15. Bresolí-Obach, R.; Torra, J.; Zanocco, R.P.; Zanocco, A.L.; Nonell, S. Singlet oxygen quantum yield determination using chemical acceptors. In Methods in Molecular Biology: Reactive oxygen species methods and protocols, 1st ed.; Espada, J. Ed.; Springer: Humana, New York, NY, **2021**; Volume 2202, pp 165-188.

16. Sharma, S.K.; Hamblin, M.R. The use of fluorescent probes to detect ROS in photodynamic therapy. In Methods in Molecular Biology: Reactive oxygen species methods and protocols, 1st ed.; Espada, J. Ed.; Springer: Humana, New York, NY, **2021**; Volume 2202, pp 215-229.

17. Dawson, J.B.; Barker, D.J.; Ellis, D.J.; Grassam, E.; Cotterill, J.A.; Fisher, G.W.; Feather, J.W. A theoretical and experimental study of light absorption and scattering by in vivo skin. *Phys. Med. Biol.* **1980**, *25*, 695–709.

18. Ntziachristos, V.; Ripoll, J.; Wang, L.V.; Weissleder R. Looking and listening to light: the evolution of whole-body photonic imaging. *Nat. Biotechnol.* **2005**, *23*, 313-320.

19. Xu, M.; Wang, L.V. Photoacoustic imaging in biomedicine. *Rev. Sci. Instrum.* **2006**, *77*, 041101.

20. Braslavsky, S.E.; Heibel, G.E. Time-resolved photothermal and photoacoustic methods applied to photoinduced processes in solution. *Chem. Rev.* **1992**, *92*, 1381–1410.

21. Gensch, T.; Viappiani, C. Time-resolved photothermal methods: accessing time-resolved thermodynamics of photoinduced processes in chemistry and biology. *Photochem. Photobiol. Sci.* **2003**, *2*, 699-721.

22. Chen, Q.; Liu, X.; Chen, J.; Zeng, J.; Cheng, Z.; Liu, Z. A self-assembled albumin-based nanoprobe for in vivo ratiometric photoacoustic pH imaging. *Adv. Mater.* **2015**, *27*, 6820–6827.

23. Weber, J.; Beard P.C.; Bohndiek, S.E. Contrast agents for molecular photoacoustic imaging. *Nat. Methods* **2016**, *13*, 639-650.

24. Knox, H.J.; Hedhli, J.; Kim, T.W.; Khalili, K.; Dobrucki, L.W.; Chan, J. A bioreducible N-oxide based probe for photoacoustic imaging of hypoxia. *Nat. Commun.* **2017**, *8*, 1794.

25. Roberts, S.; Seeger, M.; Jiang, Y.; Mishra, A.; Sigmund, F.; Stelz, A.; Lauri, A.; Symvoulidis, P.; Rolbiesky, H.; Preller, M.; Dean-Ben, L.; Razansky, D.; Orschmann, T.; Desbordes, S.C.; Vetschera, P.; Bach, T.; Ntziachristos, V.; Westmeyer, G.G. Calcium sensor for photoacoustic imaging. *J. Am. Chem. Soc.* **2018**, *140*, 2718–2721.

26. Ma, T.; Zheng, J.; Zhang, T.; Xing, D. Ratiometric photoacoustic nanoprobes for monitoring and imaging of hydrogen sulfide in vivo. *Nanoscale* **2018**, *10*, 13462–13470.

27. Pu, K.; Shuhendler, A.J.; Jokerst, J. V.; Mei, J.; Gambhir, S.S.; Bao, Z.; Rao, J. Semiconducting polymer nanoparticles as photoacoustic molecular imaging probes in living mice. *Nat. Nanotechnol.* **2014**, *9*, 233–239.

28. Zhou, E.Y.; Knox, H.J.; Reinhardt, C.J.; Partipilo, G.; Nilges, M.J.; Chan, J. Near-infrared photoactivatable nitric oxide donors with integrated photoacoustic monitoring. *J. Am. Chem. Soc.* **2018**, *140*, 11686–11697.

29. Yang, Z.; Dai, Y.; Yin, C.; Fan, Q.; Zhang, W.; Song, J.; Yu, G.; Tang, W.; Fan, W.; Yung, B.C.; Li, J.; Li, X.; Tang, Y.; Huang, W.; Song, J.; Chen, X. Activatable semiconducting theranostics: simultaneous generation and ratiometric photoacoustic imaging of reactive oxygen species in vivo. *Adv. Mater.* **2018**, *30*, 1707509.

30. Zheng, J.; Zeng, Q.; Zhang, R.; Xing, D.; Zhang, T. Dynamic-Reversible photoacoustic probe for continuous ratiometric sensing and imaging of redox status in vivo. *J. Am. Chem. Soc.* **2019**, *141*, 19226–19230.

31. Miao, Q.; Pu, K. Emerging designs of activatable photoacoustic probes for molecular imaging. *Bioconjug. Chem.* **2016**, *27*, 2808–2823.

32. Josephy, D.; Eling, T.; Mason, R. The horseradish peroxidase-catalyzed oxidation of 3,5,3′,5′-Tetramethylbenzidine. Free radical and charge-transfer complex intermediates. *J. Biol. Chem.* **1982**, *257*, 3669–3675.

33. Guo,Y.; Ma, Q.; Cao, F.; Zhao, Q.; Ji, X. Colorimetric detection of hypochlorite in tap water based on the oxidation of 3,3′,5,5′-tetramethyl benzidine. *Anal. Methods* **2015**, *7*, 4055-4058.

34. Zhang, X.; Huang, C.; Xu, S.; Chen, J.; Zeng, Y.; Wu, P.; Hou, X. Photocatalytic oxidation of TMB with the double stranded DNA–SYBR Green I complex for label-free and universal colorimetric bioassay. *Chem. Commun.* **2015**, *51*, 14465–14468.

35. Volpe, G.; Draisci, R.; Palleschi, G.; Compagnone, D. 3,3′,5,5′-Tetramethylbenzidine as electrochemical substrate for horseradish peroxidase based enzyme immunoassays. A comparative study. *Analyst* **1998**, *123*, 1303–1307.

36. Marquez, L.A.; Dunford, H.B. Mechanism of the oxidation of 3,5,3′,5′-tetramethylbenzidine by myeloperoxidase determined by transient- and steady-state kinetics. *Biochemistry* **1997**, *36*, 9349–9355.

37. Terazima, M.; Azumi, T. A time-resolved photoacoustic method with pulsed laser excitation in the condensed phase: the relation between signal intensity and decay-rate constant. *Bull. Chem. Soc. Jpn.* **1990**, *63*, 741–745.

38. Abbruzzetti, S.; Viappiani, C.; Murgida, D.H.; Erra-Balsells, R.; Bilmes, G.M. Non-toxic, water-soluble photocalorimetric reference compounds for UV and visible excitation. *Chem. Phys. Lett.* **1999**, *304*, 167–172.

39. Jankowski, J.J.; Kieber, D.J.; Mopper, K. Nitrate and Nitrite Ultraviolet Actinometers. *Photochem. Photobiol.* **1999**, *70*, 319–328.

40. Barreto, J.C.; Smith, G.S.; Strobel, N.H.; McQuillin, P.A.; Miller, T.A. Terephthalic acid: A dosimeter for the detection of hydroxyl radicals in vitro. *Life Sci.* **1994**, *56*, PL89-PL96.

41. Neckers, D.C. Rose Bengal. *J. Photochem. Photobiol. A Chem.* **1989**, *47*, 1–29.

42. Soares, A.C.; Leite, R.; Tatsuo, M.A.; Duarte, I.D. Activation of ATP-sensitive K^+ channels: mechanism of peripheral antinociceptive action of the nitric oxide donor, sodium nitroprusside. *Eur. J. Pharmacol.* **2000**, *400*, 67–71.

43. Kim, M.; Ko, S.-K.; Kim, H.; Shin, I.; Tae, J. Rhodamine cyclic hydrazide as a fluorescent probe for the detection of hydroxyl radicals. *Chem. Commun.* **2013**, *49*, 7959-7961.

44. Lin, L.; Xiao, D.; Yuan, H.; Choi, M.M.F.; Chan, W. A passive sampler for determination of nitrogen dioxide in Ambient air. *J. Chem. Educ.* **2005**, *82*, 1231-1233.

45. Mahouche-Chergui, S.; Gam-Derouich, S.; Mangeney, C.; Chehimi, M.M. Aryl diazonium salts: a new class of coupling agents for bonding polymers, biomacromolecules and nanoparticles to surfaces. *Chem. Soc. Rev.* **2011**, *40*, 4143-4166.

46. Berks, B.C.; Ferguson, S.J.; Moir, J.W.B., Richardson, D.J. Enzymes and associated electron transport systems that catalyze the respiratory reduction of nitrogen oxides and oxyanions. *Biochim. Biophys. Acta.* **1995**, *1232*, 97-173.

47. Cattaneo, M.V.; Luong, J.H.T. A water-soluble tetramethylbenzidine-2-hydroxypropyl-β-cyclodextrin inclusion complex as an efficient mediator for oxidoreductases. *Electroanalysis* **1996**, *8*, 223–228.

48. Nutting, J.E.; Rafiee, M.; Stahl, S.S. Tetramethylpiperidine N-Oxyl (TEMPO), phthalimide N-oxyl (PINO), and related N-oxyl species: electrochemical properties and their use in electrocatalytic reactions. *Chem. Rev.* **2018**, *118*, 4834-4885.

49. Armstrong, D.A.; Huie, R.E.; Koppenol, W.H.; Lymar, S.V.; Merényi, G.; Neta, P.; Ruscic, B.; Stanbury, D.M.; Steenken, S.; Wardman, P. Standard electrode potentials involving radicals in aqueous solution: inorganic radicals (IUPAC Technical Report). *Pure Appl. Chem.* **2015**, *87*, 1139-1150.

50. Khan, A.U.; Kasha, M. Singlet molecular oxygen evolution upon simple acidification of aqueous hypochlorite: Application to studies on the deleterious health effects of chlorinated drinking water. *Proc. Natl. Acad. Sci.* **1994**, *91*, 12362-12364.

51. Li, M.Y.; Cline, C.S.; Koker, E.B.; Carmichael, H.H.; Chignell, C.F.; Bilski, P. Quenching of singlet molecular oxygen ($^1O_2$) by azide anion in solvent mixtures. *Photochem. Photobiol.* **2001**, *74*, 760–764.

52. Dixon, J.K. The absorption coefficient of nitrogen dioxide in the visible spectrum. *J. Chem. Phys.* **1940**, *8*, 157-160.

53. Radi, R. Peroxynitrite, a stealthy biological oxidant. *J. Biol. Chem.* **2013**, *288*, 26464–26472.

54. Frimer, A.A.; Aljadeff, G.; Ziv, J. Reaction of (arylmethyl)amines with superoxide anion radical in aprotic media. Insights into cytokinin senescence inhibition. *J. Org. Chem.* **1983**, *48*, 1700-1705.

55. Stuehr, D.J.; Marietta, M.A. Superoxide-promoted oxidation reactions of aniline and N-methylaniline in dimethyl sulfoxide. *J. Org. Chem.* **1985**, *50*, 694-696.

56. Masuda, M.; Mower, H.F.; Pignatelli, B.; Celan, I.; Friesen, M.D.; Nishino, H.; Ohshima, H. Formation of N-nitrosamines and N-nitramines by the reaction of secondary amines with peroxynitrite and other reactive nitrogen species: comparison with nitrotyrosine formation. *Chem. Res. Toxicol.* **2000**, *13*, 301-308.

57. Shu, X.; Lev-Ram, V.; Deerinck, T.J.; Qi, Y.; Ramko, E.B.; Davidson, M.W.; Jin, Y.; Ellisman, M.H.; Tsien, R.Y. A genetically encoded tag for correlated light and electron microscopy of intact cells, tissues, and organisms. *PLoS Biol.* **2011**, *9*, e1001041.

58. Ruiz-González, R.; Cortajarena, A.L.; Mejias, S.H.; Agut, M.; Nonell, S.; Flors, C. Singlet oxygen generation by the genetically encoded tag miniSOG. *J. Am. Chem. Soc.* **2013**, *135*, 9564–9567.

59. Rodríguez-Pulido, A.; Cortajarena, A.L.; Torra, J.; Ruiz-González, R.; Nonell, S.; Flors, C. Assessing the potential of photosensitizing flavoproteins as tags for correlative microscopy. *Chem. Commun.* **2016**, *52*, 8405–8408.

60. Ragàs, X.; Agut, M.; Nonell, S. Singlet oxygen in *Escherichia coli*: new insights for antimicrobial photodynamic therapy. *Free Radic. Biol. Med.* **2010**, *49*, 770–776.

61. Bresolí-Obach, R.; Busto-Moner, L.; Muller, C.; Reina, M.; Nonell, S. NanoDCFH-DA: A silica-based nanostructured fluorogenic probe for the detection of reactive oxygen species. *Photochem. Photobiol.* **2018**, *94*, 1143–1150.